Global and Planetary Change 175 (2019) 226–237

Contents lists available at ScienceDirect

Global and Planetary Change

journal homepage: www.elsevier.com/locate/gloplacha

Extreme ENSO-driven torrential rainfalls at the southern edge of the Atacama Desert during the Late Holocene and their projection into the 21th century

Cristina Ortega[a,*], Gabriel Vargas[a], Maisa Rojas[b,c], José A. Rutllant[b,e], Práxedes Muñoz[d,e], Carina B. Lange[f,g], Silvio Pantoja[f], Laurent Dezileau[h], Luc Ortlieb[i,1]

[a] Departamento de Geología, Universidad de Chile, Santiago, Chile
[b] Deparmento de Geofísica, Universidad de Chile, Santiago, Chile
[c] Núcleo Milenio de Paleoclima, Chile
[d] Departamento de Biología Marina, Universidad Católica del Norte, Coquimbo, Chile
[e] Centro de Estudios Avanzados en Zonas Áridas (CEAZA), La Serena, Chile
[f] Departamento de Oceanografía, Centro de Investigación Oceanográfica COPAS Sur-Austral, Universidad de Concepción, Concepción, Chile
[g] Centro de Investigación Dinámica de Ecosistemas Marinos de Altas Latitudes (IDEAL), Universidad Austral de Chile, Valdivia, Chile
[h] Géosciences Montpellier, Université de Montpellier, France
[i] Sorbone Université- LOCEAN/Institut de Recherche pour le Développement (IRD), Paris, France

ARTICLE INFO

Keywords:
Extreme rainfall events
Southern edge of Atacama Desert
El Niño Southern Oscillation
Pacific South America teleconnection pattern
Pacific Decadal Oscillation
CMIP5

ABSTRACT

Extreme precipitation events and multi-annual droughts, especially in arid to semi-arid subtropical regions, are among the most critical El Niño Southern Oscillation (ENSO) and global climate change impacts. Here, we assess the variability of torrential rainfall during the Late Holocene and its projection into the 21st century at the southern edge of the hyperarid Atacama Desert.

The analysis of historical data since the beginning of the 20th century reveals that most (76.5%) alluvial disasters in the southern Atacama Desert (26–30°S) have resulted from extreme rainfall events occurring between March and September under El Niño conditions, and more frequently during the warm phase of the Pacific Decadal Oscillation. Particular rainfall events under these ocean-climate conditions are associated with the convective phase of the Madden-Julian Oscillation (MJO) near the central-equatorial Pacific, resulting in warmer sea surface temperature (SST) there and in the triggering of persistent/intense Pacific South America (PSA) tropical-extratropical teleconnection patterns which result in blocking of the westerly flow at high latitudes and the subsequent deviation of storm tracks towards central-northern Chile.

On a longer timescale, marine sediments from Tongoy Bay (30°S) reveal an increasing trend of stronger runoff by torrential coastal rain since ca. 3500 cal yr BP and even stronger heavy rainfall since ca. 1700 cal yr BP. Highly variable coastal sea surface temperatures in the same time span deduced from the sedimentary record can be explained by intensified southerly winds in connection with stronger alongshore pressure gradients and reduced coastal low-cloud cover. Both storm intensification and increased intensity of upwelling-favorable winds point to a variable climate conditioned by strengthened interannual ENSO and interdecadal ENSO-like variability during the Late Holocene.

Climate projections from the Coupled Model Intercomparison Project Phase 5 (CMIP5) indicate a reduction in annual precipitation of 15–30% during the current century, together with an intensification of the storms, such as the alluvial disaster on March 25, 2015 in Atacama.

* Corresponding author at: Departamento de Geología, Universidad de Chile, Plaza Ercilla 803, Santiago, Chile.
E-mail address: crortega@ing.uchile.cl (C. Ortega).

[1] Memorial: Luc Ortlieb was a brilliant and dedicated scientist who strongly promoted paleoclimate and geomorphology research in northern Chile. We are grateful to be part of his legacy, and will remember him as a committed naturalist, great mentor and friend.

https://doi.org/10.1016/j.gloplacha.2019.02.011
Received 15 September 2018; Received in revised form 26 January 2019; Accepted 15 February 2019
Available online 18 February 2019
0921-8181/

1. Introduction

The El Niño-Southern Oscillation (ENSO) drives dramatic precipitation anomalies, especially along the arid and semi-arid west coast of South America (e.g. Dai and Wigley, 2000), which can trigger flooding and mud flows that cause terrible disasters, loss of life and economic damage (Ward et al., 2014). Along the Atacama Desert, spanning roughly from 18° to 30°S, mean annual precipitation varies from 1 to 3 mm in the hyperarid core (e.g. 18.5–22°S) to 110 mm in the semi-arid region at 30°S. The mature stage of El Niño (warm phase of ENSO) is characterized by positive precipitation anomalies during austral summer from Ecuador to northern Peru, when strong positive sea surface temperature (SST) anomalies reach the eastern tropical Pacific. From northern to south-central Chile, positive precipitation anomalies occur during the development phase of El Niño in the previous austral winter-spring season (e.g. Curtis and Adler, 2003).

The rainfall at the southern edge of the Atacama Desert (26–30°S) strongly depends on the arrival of sporadic mid-latitude weather disturbances during austral winter-spring (Fig. 1). During El Niño, sporadic, intense precipitation events occur in this area in connection with higher frequency of persistent blocking highs west of the Antarctic Peninsula - a distinct feature of the atmospheric tropical-extratropical teleconnections (the Pacific South America – PSA pattern) (Rutllant and Fuenzalida, 1991; Mo and Higgins, 1998; Montecinos et al., 2000; Montecinos and Aceituno, 2003; Ortega et al., 2012), which drives mid-latitudes storm tracks towards central-northern Chile (Fig. 1d). To the east, during La Niña (cold phase of ENSO) the Andean Cordillera is also affected by austral summer rainfall episodes when the Bolivian High (upper level anticyclone) is localized to the southeast of the central Andes and low level north-westerly flow transports warm, moist air from the Amazon Basin (Garreaud and Aceituno, 2001).

Recently, an extreme rainfall event on March 2015 strongly impacted the southern edge of the Atacama Desert, generating a socio-natural disaster that challenged the resilience capabilities of the local communities as well as of the country (Vargas et al., 2018). This storm affected 80,000 km^2 of the Atacama region, causing violent mud and debris flows that devastated cities such as Chañaral (26°20′S) and Copiapó (27°22′S), leaving 31 dead, 16 disappeared and more than 16,000 people affected (ONEMI; Barrett et al., 2016; Bozkurt et al., 2016; Wilcox et al., 2016). Again, an event in May 2017 also impacted this region with flooding and debris flows, leaving 2 dead and more than 5000 people affected (ONEMI).

Alluvial deposits from the arid (23°S) and semiarid (32°50′S) coast of Chile show that these kinds of events occurred sporadically since the Middle Holocene (Vargas et al., 2006; Ortega et al., 2012, 2013), when a scenario of intense and persistent aridity prevailed in the central and northern coast of Chile (Villagrán and Varela, 1990; Maldonado and Villagrán, 2002, 2006; Villa-Martínez et al., 2003). An increased frequency in heavy rainfall events that generated major debris flows occurred beginning 5300–5700 yr BP and continuing over the last millennium. This marked hydrological change is recorded by terrestrial and lacustrine sediments from the north to central Chile (e.g. Jenny et al., 2003; Vargas et al., 2006; Ortega et al., 2012), and is attributed to the onset of modern tropical-extratropical teleconnection pattern

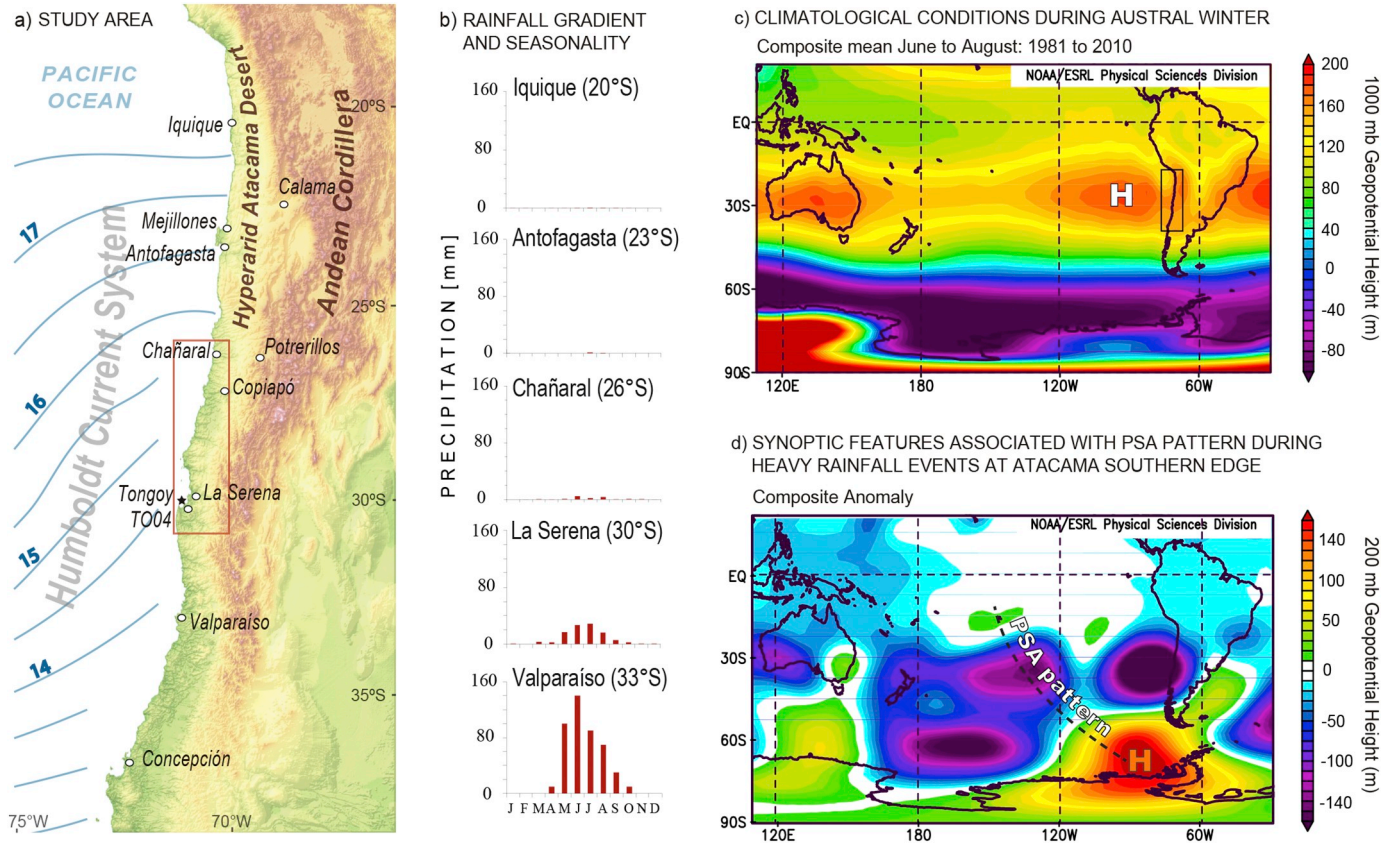

Fig. 1. a) Geomorphological and oceanographic context of the southern Atacama Desert. Black star shows the location of marine gravity core TO04 from Tongoy Bay. Mean sea surface temperature contours (1948–2011, NOAA extended SST data) for austral winter-spring are shown (blue lines). Red rectangle indicates area considered for CMIP5 model simulations. b) Seasonality pattern in rainfall and its strong latitudinal gradient along north-central Chile. c) Mean position of the Southeastern Pacific Subtropical High (white H) during austral winter. Black rectangle shows north-central Chile. d) Composite anomaly considering historical heavy rainfall events at the semi-arid coast of Chile for 10 August 1965, 13 June 1972, 24 August 1972, 17 June 1991, 12 June 1997 and 17 August 1997. Climatology period is based on 1981–2010. Note the blocking high anomaly (orange H) associated with the PSA teleconnection pattern. (For interpretation of the references to colour in this figure legend, the reader is referred to the web version of this article.)

related to ENSO variability and its strengthening (Vargas et al., 2006; Ortega et al., 2012).

Environmental reconstructions of north-central Chile (27°S − 34°S), based on pollen and pedological records, also point to more variable climate conditions during the Late Holocene. They show more frequent wet and dry periods, with alternation of erosion and soil formation in the Andes and the coastal range, which have been explained by changes in the westerly wind belt's position and/or intensity, as well as changes in the frequency of El Niño–Southern Oscillation events (Villagrán and Varela, 1990; Veit, 1996; Villa-Martinez et al., 2004: Maldonado and Villagrán, 2006; Cabré et al., 2017). Lacustrine sediment records from the subtropical Andes in north-central Chile also show a highly variable climate during the Late Holocene related to changes in precipitation and temperature (e.g. Martel-Cea et al., 2016).

Regarding the oceanographic conditions along the semiarid coast of Chile, marine sediments from 30° and 33° lat. S show a decreasing SST trend since the Middle Holocene and during the Late Holocene (Kim et al., 2002; Kaiser et al., 2008). At Los Vilos (31°50′S), isotopic data from Mesodesma Donacium records cooler coastal SST ~4–5 kyr ago compared with today (Carré et al., 2012). This points to increased coastal upwelling, suggesting an intensified Southeast Pacific Subtropical Anticyclone and a strengthened Humboldt Current System, therefore La Niña-like conditions during the Middle Holocene (Carré et al., 2012). During the Late Holocene, variable faunal assemblages, associated to increased upwelling and warmer conditions offshore Valparaiso (32°45′S), suggest intense ENSO variability since 3000 yr ago (Marchant et al., 1999). For the last millennia, marine sediments from Bahía Inglesa (27°S) show significant changes in biological productivity in response to El Niño-like conditions during ~1020–1440 cal yr BP and La Niña-like conditions during the Medieval Climate Anomaly (MCA; ~1000–500 cal yr BP) (Castillo et al., 2017). In northern Chile, the Mejillones Bay (~23°S) at the end of ~600 cal yr BP shows decreasing in biological productivity, together with increasing of subsurface oxygenation, followed by low biological productivity and slightly more oxygen concentration of dissolved oxygen of the water column, suggesting that El Niño conditions prevailed during Little Ice Age (LIA) (Guiñez et al., 2014). Further north, along the coast of Peru (~14°) an increase in biological productivity and a more intense Oxygen Minimum Zone (OMZ) in the northern section of the Humboldt Current Ecosystem suggest La Niña conditions during the MCA (Salvatteci et al., 2014). Low biological productivity together with a weak OMZ suggest El Niño-like mean state during the LIA (Salvatteci et al., 2014).

With respect to the last centuries, previous work found a change in regional ocean-climate conditions during the 19th century. The impact of El Niño appears to have been different since ca. 1817 CE, when a higher annual correlation was documented between ENSO-related heavy rainfall events occurring in austral summer in Ecuador-northern Peru and heavy rainfall during the previous austral winter-spring in central Chile (e.g. Ortlieb et al., 2002). Marine sediments from Bahía Inglesa (27°S) show an increased contribution of lithic input and variable SST since ~1820 CE, together with a reduction in the intensity of the oxygen minimum zone and biological productivity, interpreted as mixed conditions of El Niño and La Niña, suggesting this site as a transition zone in the behaviour of the Humboldt Current Ecosystem (Castillo et al., 2017). Further north, marine sediment records from Mejillones Bay (23°S) exhibit a secular change during the 19th century, interpreted as enhanced interdecadal ENSO-like variability of alongshore upwelling-favorable southerly winds, increased productivity and cooling of the coastal ocean since 1878 CE and during the 20th century, following a previous period of ocean-climate change between ~1820–1878 CE (Vargas et al., 2007). A similar ocean-atmosphere interaction change was found for the mid 1970's abrupt climate shift from the cold to the warm phase of the Pacific Decadal Oscillation (PDO) at 23°S (e.g. Rutllant et al., 1998). Marine sediments off central Peru (12–14°S) also suggest an abrupt change from a wetter to drier climate and from weaker to stronger oxygen minimum zone since ~1820 CE, followed by the strengthening of wind-driven upwelling, coastal cooling and increased productivity since 1870 CE. These changes have been tentatively explained by a northward migration of the Intertropical Convergence Zone and the Southeastern Pacific Subtropical High (SPSH), together with an intensified Walker circulation since the end of the Little Ice Age (Sifeddine et al., 2008; Gutiérrez et al., 2009; Salvatteci et al., 2014).

During the 20th century, the coast of northern Chile has suffered a persistent aridity trend, consistent with the observed and anticipated poleward expansion of the tropical belt and concurrent subtropical dry zones (Cai et al., 2012). In spite of this trend, the rainfall variability underwent pronounced fluctuations modulated by ENSO-like conditions at interannual and interdecadal time scales (Schulz et al., 2011; Quintana and Aceituno, 2012). This implies rainy years following the warm phases of ENSO, as well as consecutive rainy years and severe multi-annual droughts following PDO. Heavy rainfalls during strong to moderate El Niño events, especially during positive PDO phases, have resulted in alluvial episodes driving localized runoff in the hyperarid to semi-arid coastal Atacama Desert (Garreaud and Rutllant, 1996; Vargas et al., 2006; Ortega et al., 2012).

Despite greater consensus in projections of future global ENSO-related rainfall variability (e.g. Power et al., 2013), it is crucial to consider variations in tropical-extratropical PSA teleconnection patterns related to El Niño in order to evaluate the impact of extreme rainfall events in the arid to semi-arid regions of South America (following Mo and Higgins, 1998). Here, we analyzed meteorological data and chronicles from the southern edge of the hyperarid Atacama Desert since the beginning of 20th century (26–30°S), together with late Holocene marine sediments from Tongoy Bay (30°S; Fig. 1a) with the aim of assessing variability of extreme rainfall events and their ocean-climate conditioning factors. Finally, we complemented this information with Coupled Model Intercomparison Project 5 (CMIP5) simulations to project rainfall variability scenarios for the 21th century in this area. These simulations provide a perspective on future behavior of extreme rainfall episodes in the context of past natural variability and ongoing global climate change.

2. Site and methods

2.1. Historical data

Chronicles and observational data were exhaustively analyzed to generate a reliable and detailed record of extreme rainfall events occurred since the beginning of the 20th century. The historical information comprises the southern edge of the Atacama Desert, the Coquimbo and Atacama regions of Chile spanning between 26° and 32° lat. S. Chronicles correspond to the books and newspapers in the area, such as the books “Catástrofes de Chile” by Urrutia and Lanza (1993), “Desert trails of Atacama” by Bowman (1924), and the newspapers “El progreso de Chañaral” (1909–1955) and “El Día” of La Serena available since 1944.

Observational daily and/or monthly data were obtained from yearbooks of the Dirección Meteorológica de Chile (Chilean Weather Service) and from the compiled data book “Pluviometría de las zonas del desierto y las estepas cálidas de Chile” by Almeyda (1948). Though most of the meteorological stations present data-void periods, the station at La Serena (29°54′S, 71°12′W) has the oldest and most continuous data record of the region from 1869 to the present.

Historical heavy rainfall events were classified according to the type of damages caused in the region. In increasing order, the categories are: 'heavy rainfall events', events that caused only minor damage such as electric power cuts or fallen trees; 'flooding events', events associated to flooding in cities due to river overflowing or excess of rainfall; 'alluvial disasters', extreme rainfall events that were able to produce mud or debris flows in the region.

Monthly indices such as sea surface temperature anomalies (SSTA) in Niño 1 + 2 and Niño 3.4 regions, Southern Oscillation Index (SOI), Pacific Decadal Oscillation (PDO), Antarctic Oscillation (AAO: also known as SAM: Southern Annular Mode) were also included to assess regional atmospheric/ocean conditions during extreme torrential episodes.

Meteorological stations are scarce in the high Andes, over 2000 m a.s.l., therefore the amount of extreme rainfall events associated to the South American Monsoon is probably underestimated. Nevertheless, the aim of this research is to focus on the rains that have impacted the population of northern Chile, located mainly on the coast and its surroundings.

2.2. Marine sediment core from Tongoy Bay: proxies and geochronology

Tongoy Bay, located ca. 40 km south of La Serena (30°S), is an "upwelling shadow" area (sensu Graham and Largier, 1997), mostly protected from the direct influence of the upwelling-favorable southwest winds (e.g. Rahn et al., 2011). At the same time, it is strongly influenced by cold, nutrient-rich water advected from the adjacent coastal upwelling focus (Rutllant and Montecino, 2002). In addition, the bay receives sporadic alluvial discharge from ravines draining coastal watersheds, resulting in favorable conditions for the accumulation of both upwelling-driven biogenic remains and lithogenic material from high coastal runoff events. (Fig. 2).

Here we analyzed a 44-cm long sediment core collected at 82 m water depth in Tongoy Bay (TO04: 30°14.57′S, 71°35.99′W). The sediment core was sliced every 0.5 cm to improve high resolution geochronological model, as well as sedimentological analysis and alkenone-based SST reconstructions. The geochronological model is based on ^{210}Pb downcore activity and accelerator mass spectrometry (AMS) radiocarbon ages (Fig. 3). Mass accumulation rate from excess ^{210}Pb in the upper 7 cm ($0.087 \pm 0.012\ g\ cm^{-2}\ y^{-1}$) was determined from alpha spectrometry of its daughter ^{210}Po (Flynn, 1968). Dry sediment samples of 0.5 g were digested in several steps with a mixture of concentrated acids (HCL, HNO_3 and HF). ^{209}Po was used as a yield tracer ($2.22\ dpm\ g^{-1}$). Once the samples were totally dissolved, they were autoplated on to silver disks at ~75 °C for 2.5 h in the presence of ascorbic acid. The ^{210}Po activity was counted in a Camberra Quad alpha spectrometer, model 7404 for 24 to 48 h to achieve the desired counting statistics (4–10% 1σ errors). The activity of ^{210}Po, assumed to be in secular equilibrium with ^{210}Pb, was calculated using the ratio between natural radionuclide and the tracer, which is multiplied by the activity of the tracer at the time of plating. The delay between plating and counting produces a decay of ^{210}Po (half life: 138 days); thus, all data were corrected to the time of plating. Because of the short period elapsed between the collection date and the time of the analysis of the samples (< 4 month) compared to the half-life of ^{210}Pb (22.3 years), the calculated activities were not corrected for this delay. Calibration of AMS radiocarbon ages were performed by Intcal 13 considering a local reservoir effect ($\Delta R = 625 \pm 46$ yr), which was estimated from available ages at 4 cm depth. One of them, the age calculated (1946 CE = 4 cal yr BP) from the sedimentation rate ($SR = 0.069 \pm 0.008\ cm\ y^{-1}$) by the 210Pb excess, corresponds to 465 ± 23 yr BP, following Reimer et al. (2013). The subtraction between this age and the radiocarbon age from the organic material at the same depth (1090 ± 40 yr BP), results in 625 ± 46 yr BP, which corresponds to the local reservoir effect in Tongoy Bay. This estimation is much larger than any other ΔR estimation from the Chilean coast, nevertheless, this value represents a combined signal of continental 'old wood' effect together with the oceanic influence due to the strong upwelling processes at the adjacent Punta Lengua de Vaca area (see supplementary material).

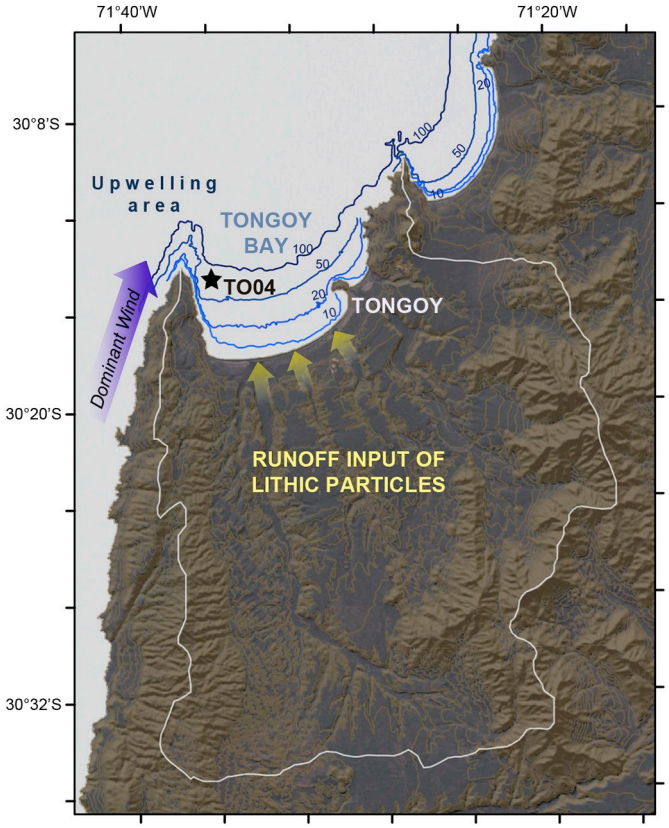

Fig. 2. Geomorphological and oceanographical setting of Tongoy Bay. Black star indicates the marine core site TO04. White line refers to the limit of the coastal watershed and yellow arrows show runoff (input of lithic particles to the coastal marine basin). Dominant wind direction and the upwelling area are also indicated. (For interpretation of the references to colour in this figure legend, the reader is referred to the web version of this article.)

Grain size distribution from sediments was measured through laser diffraction spectrometry with a Malvern Mastersizer 2000. The median of the grain size distribution is interpreted as an index of coastal runoff strength, and shows the same trends as the principal mode. Lithogenic minerals were quantified through Fourier Transformed Infrared Spectrometry with a PerkinElmer Spectrum 100 (Bertaux et al., 1998; Vargas et al., 2004). We used the flux of lithogenic minerals (quartz and plagioclase) as a proxy for runoff associated with torrential rainfall events. Alkenone-based SST reconstructions were estimated according to Prahl et al. (1988).

2.3. Projection into the 21th century

Long term climatological analysis of precipitations was based on local rain gauge data at the meteorological station of La Serena (Fig. 1a), and their comparison with CMIP5 climate model simulations (Taylor et al., 2012). We used historical simulations for the period 1850–2005 CE, forced by observed concentrations of greenhouse gases, volcanic eruptions and solar activity. Future projections follow the "Representative Concentration Pathway" 8.5 (RCP8.5) scenario corresponding to a "business as usual" emission scenario that ends with atmospheric CO_2 concentrations above 900 ppm by 2100, equivalent to a radiative forcing of $8.5\ W\ m^{-2}$. From 40 existing models, we retained 24 that reproduced the observed annual cycle of precipitation in the region (Fig. 4). Further statistical quantifications from observation and model precipitation results were carried out by calculating inter-annual and decadal variability, together with their corresponding percentages of explained variance and spectral analysis. Daily distribution of precipitation for La Serena meteorological station, historical simulations and RCP8.5 projections were also evaluated.

a)

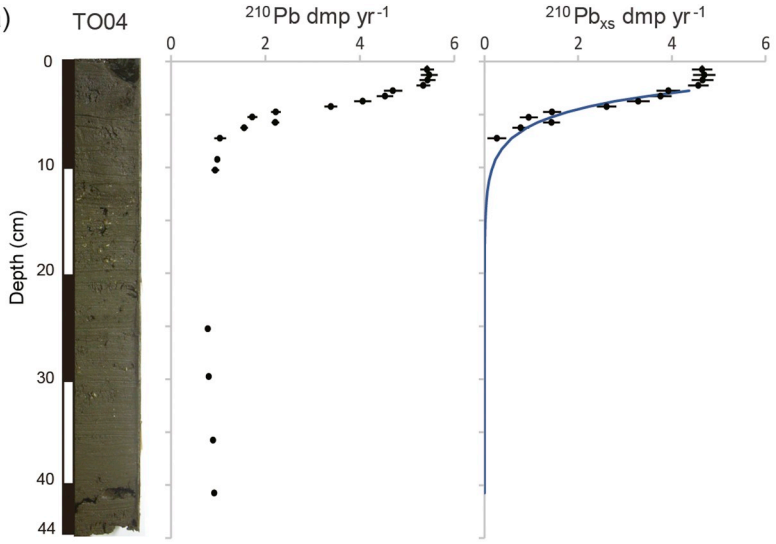

Depth (cm)	210 Pb_{xs} (dpm g^{-1})	SR (cm yr^{-1})	MAR (g cm^{-2} yr^{-1})
0.75	4.65 ± 0.22	0.069 ± 0.008	0.087 ± 0.012
1.25	4.69 ± 0.24		
1.75	4.65 ± 0.23		
2.25	4.56 ± 0.22		
2.75	3.92 ± 0.25		
3.25	3.76 ± 0.24		
3.75	3.28 ± 0.24		
4.25	2.61 ± 0.21		
4.75	1.44 ± 0.19		
5.25	0.95 ± 0.19		
5.75	1.43 ± 0.18		
6.25	0.77 ± 0.18		
7.25	0.26 ± 0.20		

Supported ^{210}Pb 0.78 ± 0.16 dpm g^{-1}

b)

Depth (cm)	Material	Laboratory Number	Age ^{14}C yr BP	Calibrated range age. (2σ). cal yr BP ΔR_{local} = 625 ± 46 yr
4	Marine sediment	Beta-247438	1090 ± 40	117 ± 116
9	Marine sediment	Beta-247439	1410 ± 40	402 ± 106
15	Marine sediment	Beta-247440	2380 ± 40	1309 ± 134
17.5	Forams (*Bolivina Plicata sp.*)	Beta-422761	2840 ± 30	1819 ± 142
24.5	Marine sediment	Beta-247241	3070 ± 40	2110 ± 173
30.5	Marine sediment	Beta-247442	3850 ± 40	3034 ± 174
38.5	Forams (*Bolivina Plicata sp.*)	Beta-422762	4370 ± 30	3684 ± 151
39	Shell (*Nuculana Cuneata sp.*)	Beta-422760	5290 ± 30	4917 ± 137
43	Marine sediment	Beta-247443	4580 ± 40	3964 ± 173

c)

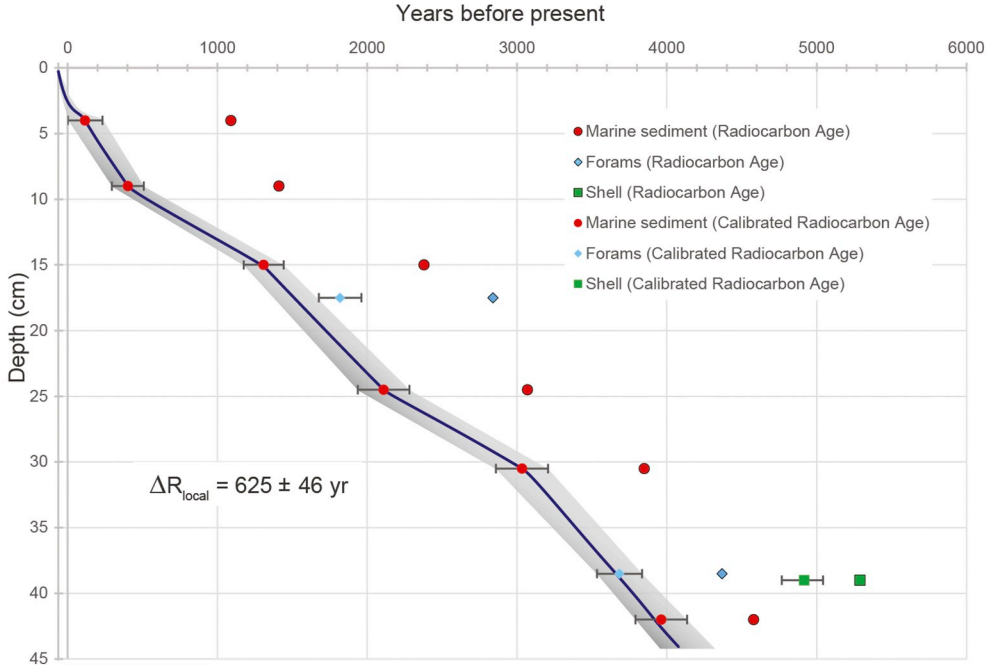

(caption on next page)

Fig. 3. Chronological model of the marine core TO04. a) ^{210}Pb and $^{210}Pb_{xs}$ downcore data. Inset table shows the unsupported ^{210}Pb values in core TO04. Sedimentation (SR) and mass accumulation rates (MAR) were estimated considering compaction according to Christensen (1982). Model: $r^2 = 0.97$. b) AMS radiocarbon dating values and calibration. c) Chronological model considering local reservoir effect ($\Delta R = 625 \pm 46$ yr).

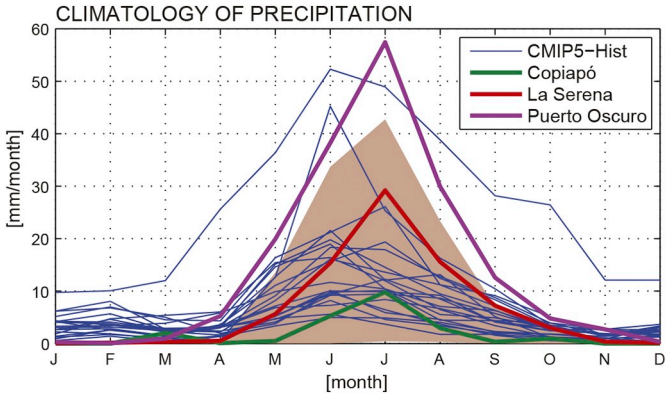

Fig. 4. Models reproducing observed annual cycle of precipitation in southern edge of Atacama.

3. Results and discussion

3.1. Extreme rainfall events since 1900

Chronicles and monthly observational data show that 52 heavy rainfall events have affected diverse localities in the southern edge of Atacama Desert area since 1900, mostly during austral fall-winter (May to August). The exceptions are two intense rainfall events in the high Andes that occurred during the austral summers (February) of 1954 and 1972 which triggered debris/mud flows, both probably related to the South American Monsoon (Fig. 5a). Another possible exception occurred in January 1906, when floodings were generated by several snow-melting events probably related to rainfall in the high Andes, with the 0 °C isotherm above the snow line.

Most of extreme rainfall events (76.5%, Fig. 5b) occurred during the negative (warm) phase of the Southern Oscillation (El Niño), in agreement with the strong relationship of heavy rainfall episodes with El Niño along the coast of Antofagasta (~23°S) (e.g. Vargas et al., 2006). Furthermore, there were more extreme rainfall events during the last warm phase (1977–1998 CE) of the Pacific Decadal Oscillation (61.5%, Fig. 5c) than in the previous cold phase (1947–1976 CE), even considering the longer duration of the latter. Therefore, we propose that the interplay between the warm phases of ENSO and PDO modulates the frequency of most of the heavy rainfall events in the southern edge of Atacama Desert.

Most of the storms (70.8%) occurred under positive SST anomalies in both the central equatorial Pacific (Niño 3.4 region) and the coastal region off Ecuador and northern Peru (Niño 1 + 2 region), suggesting that extreme rainfall events over the southern coastal Atacama Desert occur more frequently during canonical El Niño episodes (Fig. 5d). Warm SSTs in the Niño 3.4 region foster atmospheric deep convection over the central equatorial Pacific, bringing favorable conditions for triggering the Pacific South America (PSA) teleconnection pattern (Mo and Higgins, 1998). The blocking of the westerly flow by a warm-core high pressure system west of the Antarctic Peninsula, as an integral part of the PSA teleconnection pattern, results in a split polar jet-stream driving its northern branch and associated storm tracks towards the subtropics (Rutllant and Fuenzalida, 1991; Renwick, 1998). During El Niño, this occurs concomitantly with weakened trade-winds and local strengthening of the subtropical jet stream (Gallego et al., 2005), altogether enhancing the storminess of the area, which have resulted in heavy rainfalls driving floods and debris/mud flow events in the semi-arid coast of Chile (30–32°S) during the second half of 20th century (Ortega et al., 2012).

Indeed, before and during the alluvial event of March 2015, that occurred during the onset of El Niño 2015/2016 (central equatorial Pacific warming), the blocking high was particularly intense (Fig. 6) due to the superposition of El Niño conditions with a particularly strong convective phase of the Madden-Julian Oscillation (MJO) over the central equatorial Pacific (Rondanelli et al., 2019). Thus, the strong correlation between extreme rainfall events and deep convection (warm SSTs) at Niño 3.4 region suggests that the PSA teleconnection pattern was a conditioning factor for most flooding and alluvial disasters at the southern edge of the Atacama Desert during the entire 20th century and the beginning of the 21th century.

Although the blocking high over the Southeast Pacific is more frequent during austral spring and summer when the canonical El Niño occurs in conjunction with the negative phase of the Antarctic Oscillation (AAO) (Oliveira and Ambrizzi, 2017), no correlation was found between the heavy rainfall events in the Atacama Desert and the AAO (not shown). This discards the direct influence of the reduction/expansion of the zonal flow at mid-latitudes in the frequency or intensity of extreme heavy rainfall episodes at the southern edge of Atacama Desert. However, AAO-related precipitation anomalies are significant in southern Chile (largest at 42°S) and along the subtropical east coast of the continent (Gillett et al., 2006; Garreaud et al., 2009), regions where the AAO produces a strong modulation of the ENSO signal on precipitation (Garreaud et al., 2009).

In contrast with Niño 3.4 region, positive SST anomalies in Niño 1 + 2 region are not directly related to heavy rainfalls over northern Chile. Nevertheless, an anomalously warm ocean along the Peruvian coast, eventually including the Niño 1 + 2 region, seems to be a relevant factor for the intensification of storms that can finally affect the coastal Atacama Desert. During March 2015, the coast of central and southern Peru (south of El Niño 1 + 2) experienced anomalous high SSTs during the second half of the month (Bozkurt et al., 2016). This coastal ocean warming together with northwesterly winds in the lower troposphere, resulting from either a deep trough or a cutoff low aloft, led to an unusual transport of water vapor from the Peruvian coastal ocean towards the subtropical region in northern Chile. This triggered torrential rainfall and the subsequent alluvial disaster on March 24–25, 2015 (Bozkurt et al., 2016; Barrett et al., 2016). Indeed, during austral fall-winter, most heavy rainfall events (85.4%) occurred concomitantly with positive SST anomalies in the Niño 1 + 2 region, highlighting the importance of anomalous ocean warming along the coast of Ecuador and Peru as a potential water vapor source to be advected into northern Chile.

In summary, we propose that blocking highs west of Antarctic Peninsula, as a part of the PSA teleconnection pattern triggered by MJO-related deep convection at the central equatorial Pacific, and associated positive SST anomalies there, have conditioned most of the heavy rainfall events at the southern edge of Atacama Desert since the 20th century. These conditions are more intense and/or persistent when the warm phases of ENSO and PDO coincide with the convective phase of the intraseasonal MJO over the central equatorial Pacific. Hence, we propose that the interplay of these oscillations modulates the frequency of extreme rainfall events in the southern edge of Atacama Desert. On the other hand, positive SST anomalies along the Peruvian coast together with a favorable atmospheric circulation seems to be a conditioning factor for the eventual intensification of storms reaching the Atacama Desert.

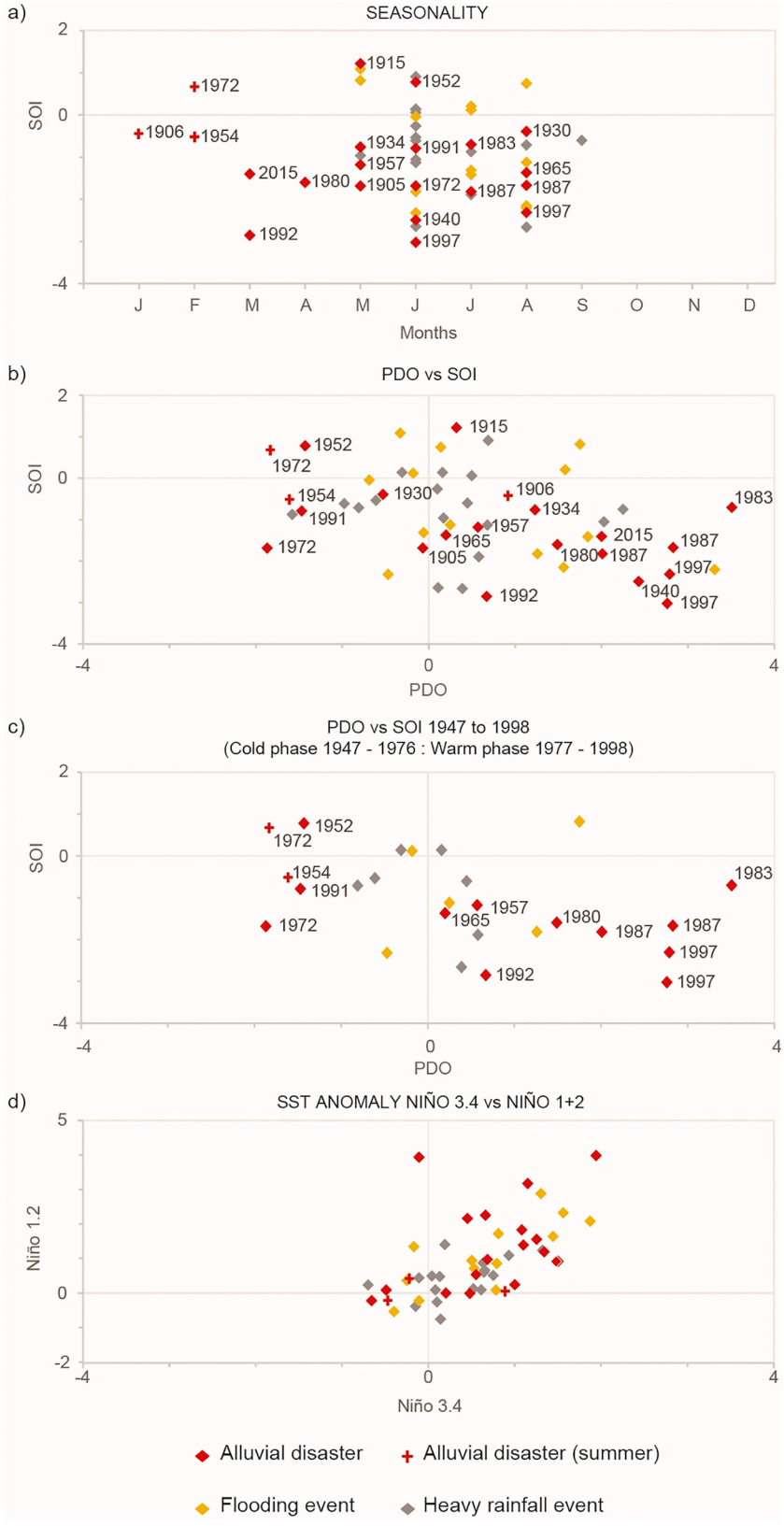

Fig. 5. Analysis of extreme rainfall events from 20th century to the present. Heavy rainfall that caused alluvial disasters at the southern edge of Atacama Desert during fall and winter (red rhombus) and during summer (red crosses); heavy rainfall that produced floods in cities (yellow rhombus) and storms associated with minor damages (gray rhombus). (a) Seasonality of heavy rainfall events. Note that most of storms have occurred during austral fall and winter. b) Distribution of extreme rainfall events with the Southern Oscillation Index (SOI) and the Pacific Decadal Oscillation (PDO). c) Distribution of extreme rainfall events with the Southern Oscillation Index (SOI) and the Pacific Decadal Oscillation (PDO), considering only the cold (1947–1976) and the warm phase (1977–1998) of the PDO. d) Monthly sea surface temperature anomalies at the Niño 3.4 and Niño 1 + 2 regions during heavy storms. (For interpretation of the references to colour in this figure legend, the reader is referred to the web version of this article.)

3.2. *Extreme rainfall events during the Late Holocene*

Sedimentological proxies in Tongoy Bay show significant millennial and multi– centennial trends during the Late Holocene. The median grain size curve shows the increasing transport capacity of sediments (grain size mean = 31 ± 4 μm) towards the sea bottom from ca. 3500 cal yr BP to ca. 1700 cal yr BP and its strengthening (grain size mean = 40 ± 3 μm) from ca. 1700 cal yr BP to ca. 200 cal yr BP (Fig. 7a). This last period is characterized by a shift in the lithic flux from relatively low values before ca. 1500 cal yr BP (mean = 43 ±

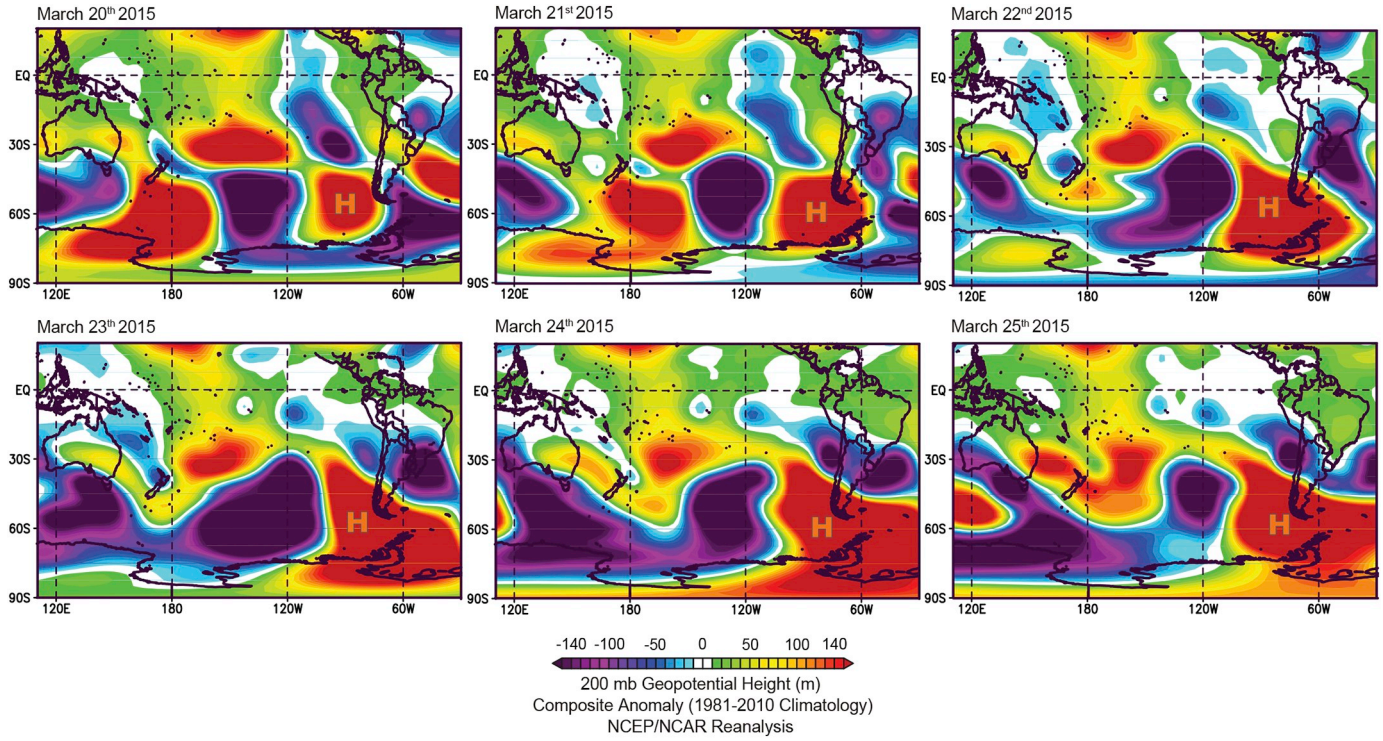

Fig. 6. Composite anomalies of 200 hPa geopotential heights before and during the extreme rainfall event of March 25th 2015. Note the persistent blocking high (H), located west of Antarctic Peninsula since March 20th 2015.

$10\,mg\,cm^{-2}\,yr^{-1}$) to higher values after ca. 1500 cal yr BP (mean = 57 ± $5\,mg\,cm^{-2}\,yr^{-1}$) (Fig. 7b). This suggests an intensification of processes supplying lithogenic material towards the coastal basin of Tongoy Bay, such as runoff from a coastal watershed associated to heavy rainfall events, and/or eolian transport. The high lithic content (30–80%) found in core TO04 (extracted ~5.6 km offshore) points to runoff as the main depositional process in most of the bay. This contrasts to other basins located further north along the hyperarid coastal Atacama Desert where lithogenic particles in marine sediments (limited to 3–15%) at similar depths are essentially of eolian origin mobilized by dominant southerly winds. Indeed, in Mejillones Bay the littoral hydrodynamic influence characterized by dominant (> 30%) detritic sediments is above 70 m b.s.l (~2 km offshore) and the marine core F981A, extracted from 75 m b.s.l (~4 km offshore), consists of 5–10% lithic particles with a confirmed eolian origin (Vargas et al., 2004, 2007; Flores-Aqueveque et al., 2014, 2015). Therefore, we can interpret two periods of strengthening of runoff associated to sporadic heavy rainfall events at the semiarid coast of Chile during the Late Holocene.

Debris flow records from Antofagasta (23°S, Vargas et al., 2006) and from Los Vilos (31°50′S, Ortega et al., 2012) also provide evidence for the impact of extreme rainfall events in the north-central Chile during the Late Holocene. In addition, the heavy rainfall trends from Tongoy (30°S) can be correlated with the Late Holocene evolution of paleoenvironmental proxies at Laguna Aculeo (33°50′S), a eutrophic lake located 400 km to the south without inflow from the Andes (e.g. Jenny et al., 2002). The intensifying runoff trend around Tongoy Bay since ca. 3500 cal yr BP is in agreement with more frequent clastic layers observed in the Laguna Aculeo sedimentary record since ca. 3200 cal yr BP, evidencing a regional impact of heavy rainfalls most probably associated with the warm phase of ENSO. Furthermore, the strengthening of heavy rainfall since ca. 1700 cal yr BP is consistent with the high lake level, where most brackish diatoms species disappeared around 1500 cal yr BP.

Chronicles of the 20th century show that most of the extreme rainfall events which impacted the southern edge of Atacama Desert are strongly linked to the PSA teleconnection, occurring more frequently and/or persisting longer during warm ENSO and ENSO-like conditions. Therefore, we propose that the Late Holocene increased runoff trends, interpreted as intensified heavy rainfall events, suggest stronger El Niño episodes since ca. 3500 cal yr BP, further strengthened since ca. 1700 cal yr BP.

Highly variable SSTs in Tongoy Bay occurred during the last 2000 years (Fig. 7c), and possibly earlier, in agreement with variable upwelling since ~3000 years ago suggested by variable faunal assemblages (32°45′S) (Marchant et al., 1999). This high variability contrasts with the sustained cooling trend in the warmer offshore SSTs (Fig. 7d, Kim et al., 2002; Kaiser et al., 2008) pointing to the strong influence of the upwelling processes in the bay during the Late Holocene. This can be a consequence of strengthened coastal southerly wind periods which resulted in higher marine phytoplankton productivity, as it is suggested by the alkenone content from Tongoy Bay (supplementary material). We propose that periods of intensified (i.e. coastal southerlies and southeasterly trades) have resulted from stronger alongshore pressure gradients and associated low-cloud cover, pointing to marked La Niña episodes during the Late Holocene.

The difference between coastal and offshore temperature trends at Tongoy (30°S) during the Late Holocene ranges between 3 and 5 °C, whereas such difference at Los Vilos (31°50′S) would range between 3 and 4 °C for the Middle Holocene, according to Carré et al. (2012). This suggests that similar or slightly stronger upwelling-favorable winds affected the semiarid subtropical coast during the Late Holocene, in comparison with the Middle Holocene, supporting the occurrence of intense La Niña episodes during this period.

Although the coastal SST off Tongoy (30°S) is more variable than the coastal SST off Bahía Inglesa (27°S; Castillo et al., 2017), probably due to the major impact of upwelling near Punta Lengua de Vaca, both curves show a similar trend during the last millennium, pointing to cooler coastal waters on average during the Medieval Climate Anomaly. Nevertheless, the high runoff recorded at Tongoy Bay contrasts with the lower input of lithic particles at Bahía Inglesa during this period, possibly due to the different geomorphological characteristics of the

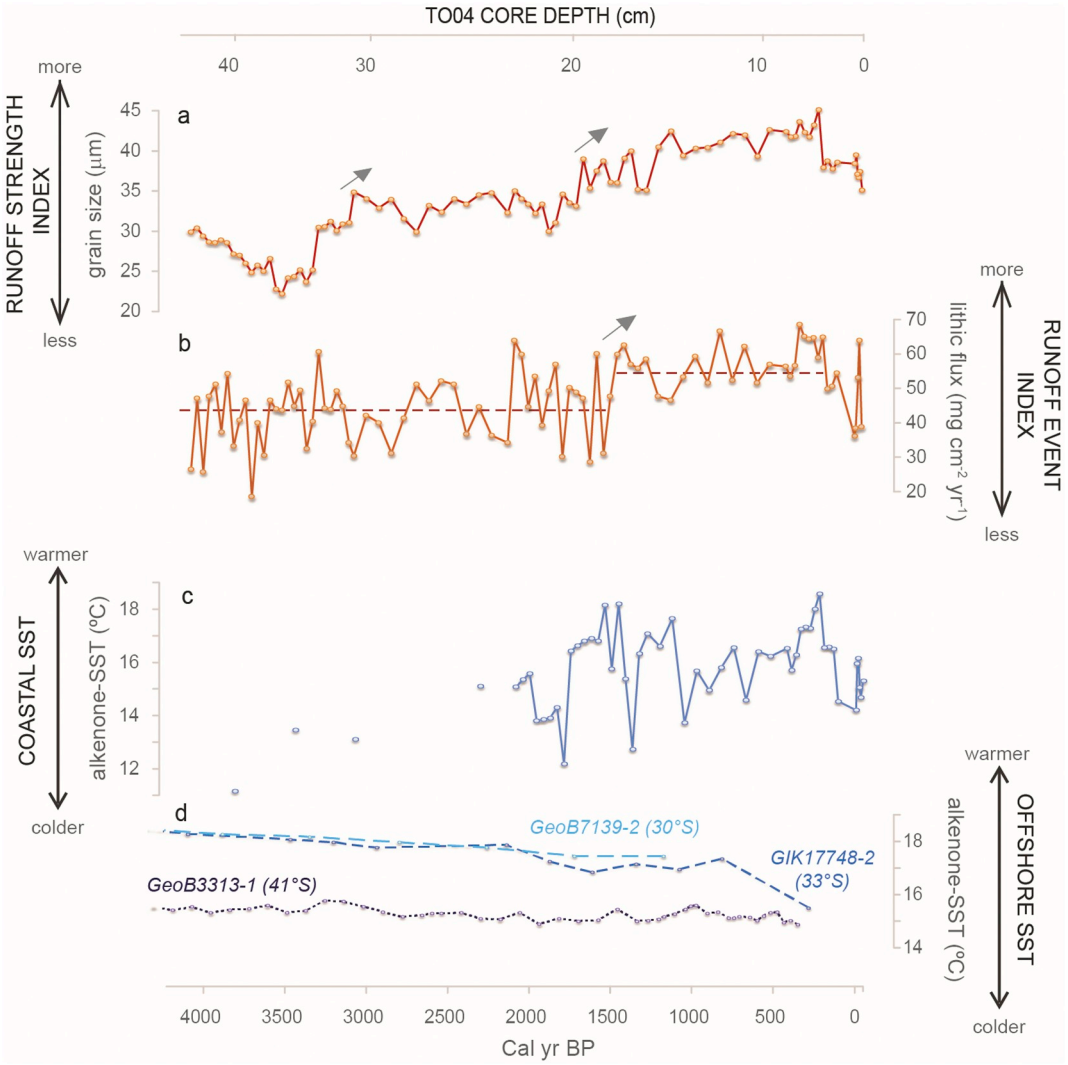

Fig. 7. Sedimentary proxies from core TO04 (Tongoy Bay, 30°S). a) Grain size variations (represented by its median), used as a proxy for coastal runoff strength. Note the increasing trend in grain size at ca. 3500 cal yr BP and ca. 1700 cal yr BP. b) Coastal runoff index based on the reconstructed flux of lithic minerals (quartz and albite). Brown horizontal lines show lithic flux average before and after ca. 1700 cal yr BP. Black arrows mark the hydrological shifts. c) Reconstructed sea surface temperature (SST) based on alkenones showing highly variable temperature in Tongoy Bay during the last ca. 2000 years, associated with variable upwelling during the Late Holocene. d) Alkenone-derived SST offshore at 30°S (Kaiser et al., 2008), 33°S (Kim et al., 2002; Ortlieb et al., 2011) and 41°S (Lamy et al. 2002). (For interpretation of the references to colour in this figure legend, the reader is referred to the web version of this article.)

adjacent catchments. Warmer SSTs at the eastern equatorial Pacific during the Late Holocene (Koutavas et al., 2002; Koutavas et al., 2006; Rustic et al., 2015) are in agreement with the high lithic runoff associated with strong rainfall events at Tongoy in connection with El Niño episodes.

In summary, the southern edge of Atacama Desert has been affected by the increase in intensity of the sporadic heavy rainfall events alternating with periods of intense southerly winds during the Late Holocene. We propose that the occurrence of these two processes has resulted because of the high variability of ENSO and ENSO-like conditions during the Late Holocene, including tropical-extratropical teleconnections patterns that result in strong effects along the coastal Atacama Desert in northern Chile.

In general, paleoclimate records from eastern North Pacific (Barron and Anderson, 2011), western equatorial Pacific (Stott et al., 2004), eastern equatorial Pacific records (Koutavas et al., 2006; Koutavas et al., 2002; Conroy et al., 2009) and El Niño frequency and intensity, as modeled by Clement et al. (2000) are in agreement with the high variability of ENSO during the Late Holocene suggested by the runoff strength and coastal SST proxies in TO04 core.

3.3. Future scenarios from CMIP5 model simulations

Observed standardized annual precipitation and the 10-year running average at La Serena show a general decreasing trend (Fig. 8a) reflecting a persistent aridification affecting the semi-arid coast of Chile. The linear trend over the whole observed period (1869–2016 CE) indicates that La Serena has had a 4% decrease in precipitation per decade (Fig. 8a), as previously documented by Schulz et al. (2011) and Quintana and Aceituno (2012). A similar calculation for CMIP5 simulations (1850–2005, *historical* simulations) indicates no significant trend over the 20th century. This difference between observations and simulations suggests that most of the observed trend is due to natural variability instead of a forced response to anthropogenic forcing. If this is the case, it is normal that the models do not reproduce the exact natural, internal variability of the climate over this period. On the other hand, for the future (using CMIP5 *RCP8.5* simulations), the models project about a 3% per decade rainfall decrease for the 21st century in the mean (Figs. 8b and 9a). This would lead to a 15–30% decrease in precipitation by the end of the current century, hence projecting the continuity of desertification along the southern edge of Atacama Desert.

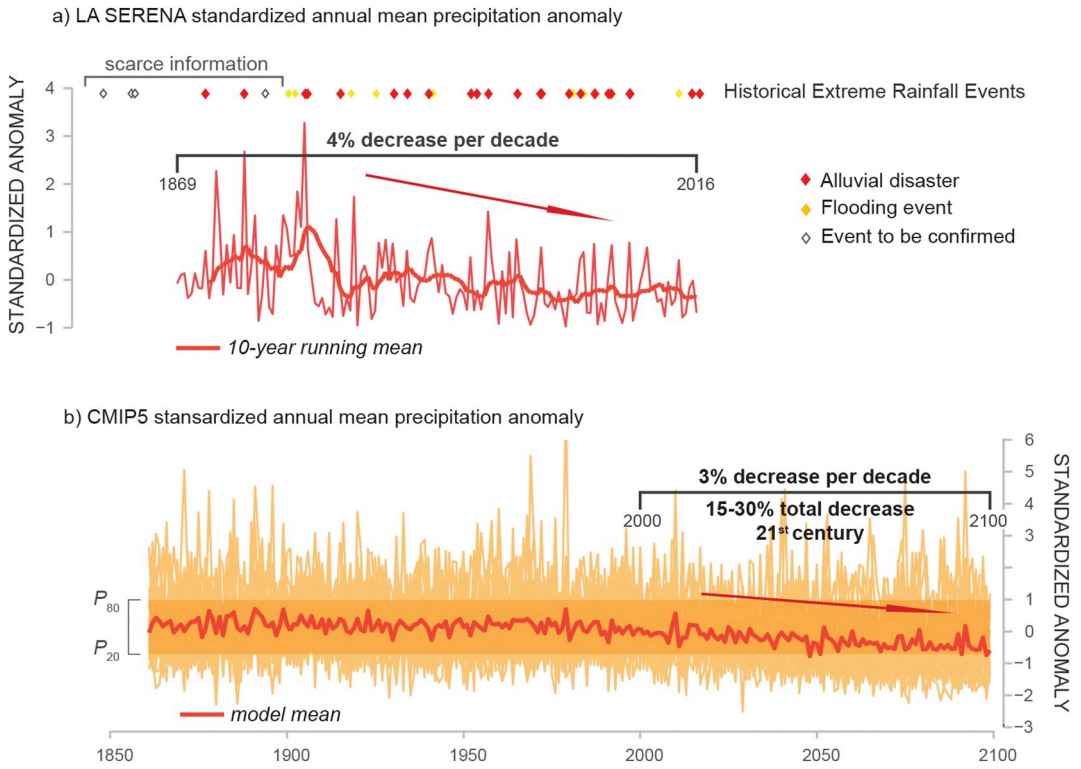

Fig. 8. Comparison between observed precipitation and CMIP5 long-term model results. a) Historical annual rainfall anomaly at La Serena standardized by annual mean precipitation and a 10-year running mean (thin and thick red lines, respectively). Note, historical extreme rainfall events (rhombus) have occurred regardless the annual rainfall decrease tendency. b) CMIP5 annual rainfall anomaly, given by standardized precipitation obtained from model simulations (thin orange lines), 20–80th percentile range (orange bar), and model mean (thick orange line). A decreasing trend of annual rainfall is estimated for the rest of the 21st century. (For interpretation of the references to colour in this figure legend, the reader is referred to the web version of this article.)

Historical extreme rainfall events at the southern edge of the Atacama Desert have occurred regardless of the negative trend in annual precipitation during the last centuries (Fig. 8a). At the daily timescale, rainfall days in this semi-arid region represent only 4% of the year and this value is projected to decrease to 2% by the end of the century (Fig. 9b). However, for the rainfall days, the 99 percentile during the period 1961–1990 CE corresponds to 60 mm day^{-1}, whereas the 99 percentile over the period 2070–2099 CE would increase to 69 mm day^{-1} (Fig. 9b). Note that the other percentiles (median, 20th, 80th) do not show any significant change in intensity. Therefore, the region is projected to become drier, but with more intense extreme rainfall events, such as the one that occurred in March 2015. This pattern follows the conceptual model of global warming related to precipitation changes (Rajah et al., 2014).

Spectral analysis of La Serena precipitation time series indicates clear inter-annual as well as decadal to multi-decadal variability, with a spectral peak at ca. 18 years (not shown), similar to the PDO. Most of CMIP5 simulations revealed inter-annual and decadal variability similar to our observations, representing about 35 and 5% of the total variance, respectively (Fig. 9c). Calculations for the 21st century from RCP8.5 simulations indicate no significant changes throughout this period, discarding statistically significant changes in inter-annual and decadal variability related to ENSO and ENSO-like conditions in the models.

In summary, aridification along the semi-arid coast of Chile is projected to continue during the 21st century regardless of ENSO activity, consistent with global warming trend, the expected widening of the Hadley Cell and concomitant expansion of the subtropical dry zones (Johanson and Fu, 2009; Cai et al., 2012; Scheff and Frierson, 2012). Stronger extreme rainfall events are also expected, whose frequency will continue to be modulated by ENSO and ENSO-like conditions as during the last centuries.

4. Concluding remarks

The southern edge of Atacama Desert has been impacted by more than 50 heavy rainfall events since the 20th century. Ninety-eight percent of these storms occurred during austral fall-winter, and more than 60% of them had devastating effects in several Chilean cities.

Our analysis of chronicles and observational data compiled since the 20th century shows that most of the extreme rainfall events have occurred during canonical El Niño events. We propose that blocking of the westerlies by slow-drifting warm core anticyclones west of the Antarctic Peninsula, as an integral part of the PSA teleconnection pattern, is fostered by MJO-related deep convection at central equatorial Pacific. There the associated positive SST anomalies resulting from surface convergence are enhanced during the warm phases of ENSO and PDO. Altogether, these atmospheric circulation anomalies constitute a conditioning factor for heavy rainfall events over the southern edge of the Atacama Desert.

Heavy rainfall events have also impacted the southern edge of the Atacama Desert during the Late Holocene. Sedimentological proxies from Tongoy Bay (30°S) show an intensification of torrential rainfall episodes since ca. 3500 cal yr BP, suggesting more intense/persistent PSA teleconnection patterns associated with positive SST anomalies and with more favorable convective conditions in the central equatorial Pacific during the Late Holocene. Furthermore, highly variable upwelling at least since ca. 2000 cal yr BP, suggests strengthened equatorward winds associated with stronger alongshore pressure gradients and reduced coastal low-cloud cover during the Late Holocene. Thus, these two processes affecting the southern edge of the Atacama Desert point to the strengthening of the variability in ENSO and ENSO-like conditions during the same time period.

Climate change projections following the RCP8.5 emission scenario, point to a 15–30% decrease in annual precipitation, thus contributing

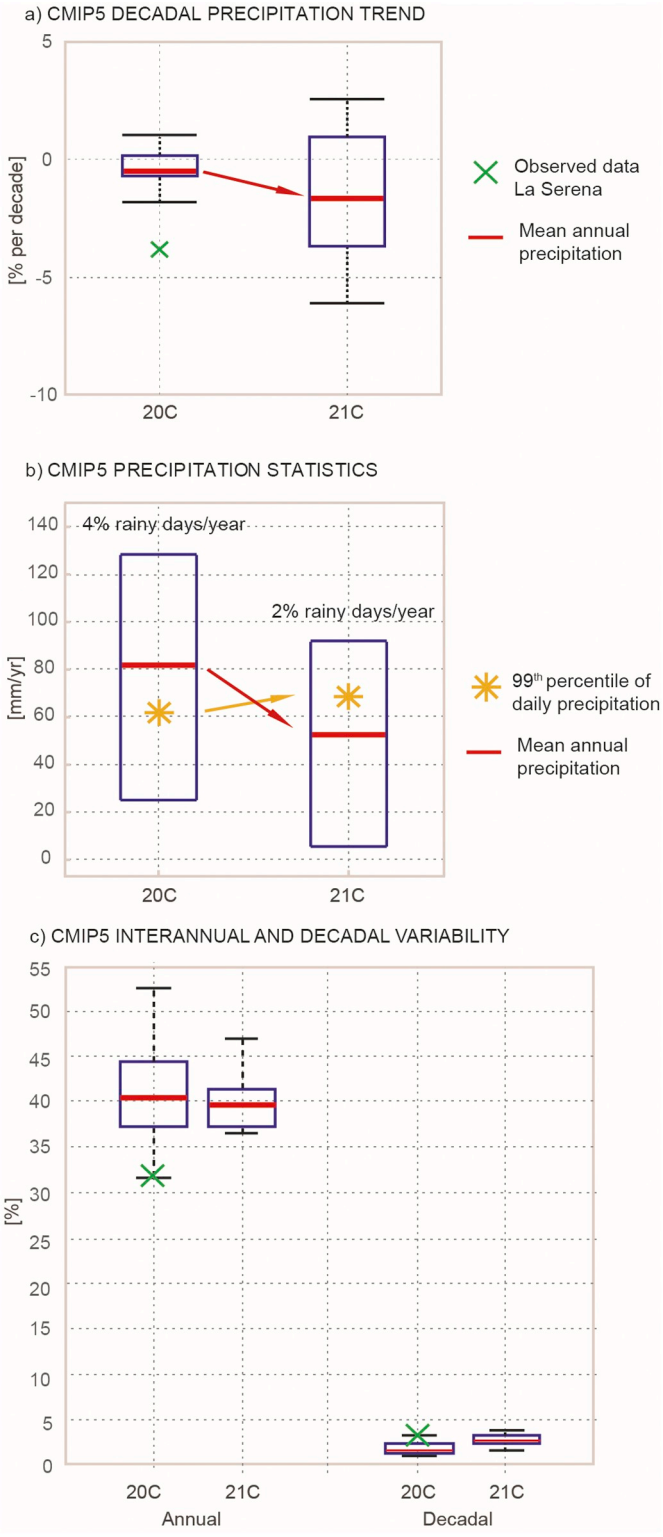

Fig. 9. Decreasing trend of rainfall and more intense storms projected to the 21st century by CMIP5. Mean annual precipitation for La Serena (red bar) and 20th and 80th percentiles (box limits) for the 1961–1990 period (left boxes corresponding to 20th century) and 2070–2099 (right boxes corresponding to 21st century). Mean annual rainfall for La Serena by observational data (green cross). a) Decadal precipitation trend. b) Rainfall statistics. Yellow stars correspond to the 99th percentile of daily precipitation; and 4% and 2% are days with rainfall in the two periods considered. c) Interannual and decadal variability. (For interpretation of the references to colour in this figure legend, the reader is referred to the web version of this article.)

to the ongoing aridification trend of the southern Atacama Desert towards the end of the 21st century. This is consistent with the widening of the Hadley Cell and the poleward expansion of the subtropical dry zones, as an outcome of global warming. Superimposed on this climate scenario, stronger rainfall events modulated by ENSO and ENSO-like conditions will also impact this arid to semiarid region. Therefore, territorial planning and mitigation measures that work in the long term are essential to avoid disastrous consequences.

Acknowledgements

This work was funded by FONDECYT #11060484 (GV), CONICYT doctoral grant and FONDECYT #3150706 (CO), FONDECYT #1171773 (MR), NC120066 and FONDAP-CONICYT 15110009 (MR), FONDAP-CONICYT 15010007 and COPAS Sur-Austral CONICYT PIA APOYO CCTE AFB170006 (SP and CBL). We acknowledge Hugues Boucher and Abdel Sifeddine (LOCEAN, France) for providing additional mineralogical data, and the support of the Hanse-Wissenschaftskolleg (Hanse Institute for Advanced Studies), Delmenhorst, Germany (CBL and SP). We thank to the captain and crew of the R/V Stella Maris from Universidad Católica del Norte, for their support during fieldwork in 2004. We aknowledge to Seth Saltiel, Carolina Muñoz and Fernando Sepúlveda for their comments to improve the manuscript. We also thank valuable comments from the editor and anonymous reviewers.

Appendix A. Supplementary data

Supplementary data to this article can be found online at https://doi.org/10.1016/j.gloplacha.2019.02.011.

References

Barrett, B.S., Campos, D.A., Vicencio Veloso, J., Rondanelli, R., 2016. Extreme temperatura and precipitation events in March 2015 in central and northern Chile. J. Geophys. Res. Atmos. 121, 4563–4580. https://doi.org/10.1002/2016JD024835.

Barron, J.A., Anderson, L., 2011. Enhanced Late Holocene ENSO/PDO expression along the margins of the eastern North Pacific. Quat. Int. 235, 3–12.

Bertaux, J., Frohlich, F., Ildefonse, Ph., 1998. Multicomponent analysis of FTIR spectra: quantification of amorphous silica and crystallized mineral phases in synthetic and natural sediments. J. Sediment. Res. 68 (3), 440–447.

Bozkurt, D., Rondanelli, R., Garreaud, R., Arriagada, A., 2016. Impact of warmer eastern tropical Pacific SST on the March 2015 Atacama floods. Mon. Weather Rev. 144, 4441–4460.

Cabré, A., Aguilar, G., Riquelme, R., 2017. Holocene evolution and geochronology of a semiarid fluvial system in the western slope of the Central Andes: AMS ^{14}C data in El Tránsito River Valley, Northern Chile. Quat. Int. 438, 20–32.

Cai, W., Lengaigne, M., Borlace, S., Collins, M., Cowan, T., McPhaden, M.J., Timmermann, A., Power, S., Brown, J., Menkes, C., Ngari, A., Vincent, E.M., Widlansky, M.J., 2012. More extreme swings of the South Pacific convergence zone due to greenhouse warming. Nature 488, 365–369.

Carré, M., Azzoug, M., Bentaleb, I., Chase, B.M., Fontugne, M., Jackson, D., Ledru, M.-P., Maldonado, A., Sachs, J.P., Schauer, A.J., 2012. Mid-Holocene mean climate in the South-Eastern Pacific and its influence on South America. Quat. Int. 253, 55–66. https://doi.org/10.1016/j.quaint.2011.02.004.

Castillo, A., Valdés, J., Sifeddine, A., Reyss, J.L., Bouloubassi, I., Ortlieb, L., 2017. Changes in biological productivity and ocean-climatic fluctuations during the last ~ 1.5 kyr in the Humboldt ecosystem off northern Chile (27°S): a multiproxy approach. Palaeogeogr. Palaeoclimatol. Palaeoecol. 485, 798–815. https://doi.org/10.1016/j.palaeo.2017.07.038.

Christensen, E.R., 1982. A model for radionuclides in sediments influenced by mixing and compaction. J. Geophys. Res. 87 (C1), 566–572.

Clement, A.C., Seager, R., Cane, M.A., 2000. Suppression of El Niño during the mid-Holocene by changes in the Earth's orbit. Paleoceanography 15, 731–737.

Conroy, J.L., Restrepo, A., Overpeck, J.T., Steinitz-Kannan, M., Cole, J.E., Bush, M.B., Colinvaux, P.A., 2009. Unprecedented recent warming of surface temperatures in the eastern tropical Pacific Ocean. Nat. Geosci. 2, 46–50.

Curtis, S., Adler, R., 2003. Evolution of El Niño–precipitation relationships from satellites and gauges. J. Geophys. Res. 108 (D4), 4153. https://doi.org/10.1029/2002JD002690.

Dai, A., Wigley, T.M.L., 2000. Global patterns of ENSO-induced precipitation. Geophys. Res. Lett. 27 (9), 1283–1286.

Flores-Aqueveque, V., Alfaro, S., Vargas, G., Caquineau, S., Valdés, J., 2014. Assessing the origin and variability of eolian lithic material for high-resolution paleoceanographic reconstructions off northern Chile. J. Sediment. Res. 84 (10), 897–909.

Flores-Aqueveque, V., Alfaro, S., Vargas, G., Rutllant, J.A., Caquineau, S., 2015. Aeolian particles in marine cores as a tool for quantitative high-resolution reconstruction of

upwelling favorable winds along coastal Atacama Desert, Northern Chile. Prog. Oceanogr. 134, 244–255.
Flynn, W.W., 1968. The determination of low levels of Polonium 210 in environmental materials. Anal. Chem. Acta 43, 221–227.
Gallego, D., Ribera, P., Garcia-Herrera, R., Hernandez, E., Gimeno, L., 2005. A new look for the Southern Hemisphere jet stream. Clim. Dyn. 24, 607–621.
Garreaud, R., Aceituno, P., 2001. Interannual rainfall variability over the South American Altiplano. J. Clim. 14 (12), 2779–2789. https://doi.org/10.1175/1520-0442(2001)014<2779:IRVOTS>2.0.CO;2.
Garreaud, R., Rutllant, J.A., 1996. Análisis meteorológico de los aluviones de Antofagasta y Santiago de Chile en el periodo 1991–1993. Atmósfera 9, 251–271.
Garreaud, R., Vuille, M., Campagnucci, R., Marengo, J., 2009. Present–day south American climate. Palaeogeogr. Palaeoclimatol. Palaeoecol. 281, 180–195. https://doi.org/10.1016/j.paleo.2007.10.032. Special issue (LOTRED South America).
Gillett, N.P., Kell, T.D., Jones, P.D., 2006. Regional climate impacts of the southern annular mode. Geophys. Res. Lett. 33, L23704. https://doi.org/10.1029/2006GL027721.
Graham, W.M., Largier, J.L., 1997. Upwelling shadows as nearshore retention sites: the example of Monterrey Bay. Cont. Shelf Res. 17, 509–532.
Guiñez, M., Valdés, J., Sifeddine, A., Boussafir, M., Dávila, P., 2014. Anchovy Population and ocean-climatic fluctuations in the Humboldt Current System during the last 700 years and their implications. Palaeogeogr. Palaeoclimatol. Palaeoecol. 415, 210–224.
Gutiérrez, D., Sifeddine, A., Field, D.B., Ortlieb, L., Vargas, G., Chávez, F.P., Velazco, F., Ferreira, V., Tapia, P., Savatteci, R., Boucher, H., Morales, M.C., Valdés, J., Reyss, J.-L., Campusano, A., Boussafir, M., Mandeng-Yogo, M., García, M., Baumgartner, T., 2009. Rapid reorganization in ocean biogeochemistry off Peru towards the end of the Little Ice Age. Biogeosciences 6, 835–848. https://doi.org/10.5194/bg-6-835-2009.
Jenny, B., Valero-Garcés, B.L., Villa-Martinez, R., Urrutia, R., Geyh, M.A., Veit, H., 2002. Early to mid-Holocene aridity in Central Chile and the southern westerlies: the Aculeo Lake record (34°S). Quat. Res. 58, 160–170.
Jenny, B., Wilhem, D., Valero-Garcés, B.L., 2003. The Southern Westerlies in Central Chile: Holocene precipitation estimates based on a water balance model for Laguna Aculeo (33°50′S). Clim. Dyn. 20 (2), 269–280.
Johanson, C.M., Fu, Q., 2009. Hadley cell widening: model simulations versus observations. J. Clim. 22, 2713–2725.
Kaiser, J., Schefub, E., Lamy, F., Mohtadi, M., Hebbeln, D., 2008. Glacial to Holocene changes in sea surface temperature and coastal vegetation in north Central Chile: high versus low latitude forcing. Quat. Sci. Rev. 27, 2064–2075.
Kim, J.-H., Schneider, R.R., Hebbeln, D., Müller, P.J., Wefer, G., 2002. Last deglacial sea surface temperature evolution in the Southeast Pacific compared to climate changes on the south American continent. Quat. Sci. Rev. 21, 2085–2097.
Koutavas, A., Lynch-Stieglitz, J., Marchitto Jr., T.M., Sachs, J.P., 2002. El Niño-like pattern in ice age tropical sea surface temperature. Science 297, 226–230.
Koutavas, A., de Menocal, P.B., Olive, G.C., Lynch-Stieglitz, J., 2006. Mid-Holocene El Niño-Southern Oscillation (ENSO) attenuation revealed by individual foraminifera in eastern tropical Pacific sediments. Geology 34, 993–996.
Lamy, F., Rühlemann, C., Hebbeln, D., Wefer, G., 2002. High- and low-latitude climate control on the position of the southern Peru–Chile current during the Holocene. Paleoceanography 17 (2), 1028. https://doi.org/10.1029/2001PA000727.
Maldonado, A., Villagrán, C., 2002. Paleoenvironmental changes in the semiarid coast of Chile (~32°S) during the last 6200 cal years inferred from a swampforest pollen record. Quat. Res. 58, 130–138.
Maldonado, A., Villagrán, C., 2006. Climate variability over the last 9900 cal yr BP from a swamp forest pollen record along the semiarid coast of Chile. Quat. Res. 66, 246–258.
Marchant, M., Hebbeln, D., Wefer, G., 1999. High resolution plancktic foraminiferal record of the last 13,300 years from the upwelling area off Chile. Mar. Geol. 161, 115–128.
Martel-Cea, A., Maldonado, A., Grosjean, M., Alvial, I., de Jong, R., Fritz, S.C., von Gunten, L., 2016. Late Holocene environmental changes as recorded in the sediments of high Andean Laguna Chepical, Central Chile (32°S;3050 m a.s.l.). Palaeogeogr. Palaeoclimatol. Palaeoecol. 461, 44–54.
Mo, K.C., Higgins, R.M., 1998. The Pacific–South American modes and tropical convection during the Southern Hemisphere winter. Mon. Weather Rev. 126, 1581–1596.
Montecinos, A., Aceituno, P., 2003. Seasonality of the ENSO-related rainfall variability in Central Chile and associated circulation anomalies. J. Clim. 16, 281–296.
Montecinos, A., Díaz, A., Aceituno, P., 2000. Seasonal diagnostic and predictability of rainfall in subtropical South America based on tropical Pacific SST. J. Clim. 13, 746–758.
Oliveira, F., Ambrizzi, T., 2017. The effects of ENSO-types and SAM on the large-scale southern blockings. Int. J. Climatol. 37, 3067–3081.
ONEMI Oficina Nacional de Emergencia del Ministerio del Interior. www.onemi.cl/noticias.
Ortega, C., Vargas, G., Rutllant, J.A., Jackson, D., Méndez, C., 2012. Major hydrological regime change along the semi-arid western coast of South America during the early Holocene. Quat. Res. 78, 513–527.
Ortega, C., Vargas, G., Rutllant, J., 2013. Major hydrological regime change along the semiarid western coast of South America during the early Holocene – response to comments by Maldonado and Moreiras. Quat. Res. 80, 140–142.
Ortlieb, L., Vargas, G., Hocquenghem, A.M., 2002. ENSO reconstruction based in documentary data from Ecuador, Peru and Chile. PAGES Newsl. 10, 14–17.
Ortlieb, L., Vargas, G., Saliège, J,-F., 2011. Marine radiocarbon reservoir effect along the northern Chile-southern Peru coast (14–24°S) throughout the Holocene. Quat. Res. 75, 91–103.
Power, S., Delage, F., Chung, C., Kociuba, G., Keay, K., 2013. Robust twent-first-century projections of El Niño and related precipitation variability. Nature 502, 541–545. https://doi.org/10.1038/nature12580.
Prahl, F.G., Muehlhausen, L.A., Zahnle, D., 1988. Further evaluation of long–chain alkenones as indicators of paleoceanographic conditions. Geochim. Cosmochim. Acta 52, 2303–2310.
Quintana, J.M., Aceituno, P., 2012. Changes in the rainfall regime along the extratropical west coast of South America (Chile): 30°–43°S. Atmósfera 25 (1), 1–22.
Rahn, D., Garreaud, R., Rutllant, J., 2011. The low-level atmospheric circulation near Tongoy Bay / point Lengua de Vaca (Chilean coast, 30°S). Mon. Weather Rev. 139, 3628–3647. https://doi.org/10.1175/MWR-D-11-00059.1.
Rajah, K., O'Leary, T., Turner, A., Petrakis, G., Leonard, M., Westra, S., 2014. Changes to the temporal distribution of daily precipitation. Geophys. Res. Lett. 41. https://doi.org/10.1002/2014GL062156.
Reimer, P.J., Bard, E., Bayliss, A., Beck, J.W., Blackwell, P.G., Bronk Ramsey, C., Buck, C.E., Cheng, H., Edwards, R.L., Friedrich, M., Grootes, P.M., Guilderson, T.P., Haflidason, H., Hajdas, I., Hatté, C., Heaton, T.J., Hoffmann, D.L., Hogg, A.G., Hughen, K.A., Kaiser, K.F., Kromer, B., Manning, S.W., Niu, M., Reimer, R.W., Richards, D.A., Scott, E.M., Southon, J.R., Staff, R.A., Turney, C.S.M., van der Plicht, J., 2013. IntCal13 and Marine13 radiocarbon age calibration curves 0–50,000 years cal BP. Radiocarbon 55 (4), 1869–1887.
Renwick, J., 1998. ENSO-related variability in the frequency of South Pacific blocking. Mon. Weather Rev. 126, 3117–3123.
Rondanelli, R., Hatchett, B., Rutllant, J.A., Bozkurt, D., Garreaud, R., 2019. Strongest MJO on Record Triggers Extreme Atacama Rainfall and Warmth in Antarctica. https://doi.org/10.1029/2018GL081475.
Rustic, G.T., Koutavas, A., Marchitto, T.M., Linsley, B.K., 2015. Dynamical excitation of the tropical Pacific Ocean and ENSO variabilityby Little Ice Age cooling. Science 350, 1537–1541.
Rutllant, J., Fuenzalida, H., 1991. Synoptic aspects of the Central Chile rainfall variability associated with the Southern Oscillation. Int. J. Climatol. 11, 67–76.
Rutllant, J.A., Montecino, V., 2002. Multiscale upwelling forcing cycles and biological response off North–Central Chile. Rev. Chil. Hist. Nat. 75, 217–231.
Rutllant, J., Fuenzalida, H., Torres, R., Figueroa, D., 1998. Interacción océano-atmósfera-tierra en la Región de Antofagasta (Chile, 23°S): Experimento DICLIMA. Rev. Chil. Hist. Nat. 71, 405–427.
Salvatteci, R., Gutiérrez, D., Field, D., Sifeddine, A., Ortlieb, L., Bouloubassi, I., Boussafir, M., Boucher, H., Cetin, F., 2014. The response of the Peruvian Upwelling Ecosystem to centennial-scale global change during the last two millennia. Clim. Past 10, 715–731. https://doi.org/10.5194/cp-10-715-2014.
Scheff, J., Frierson, D., 2012. Twenty-first-century multimodel subtropical precipitation decline are mostly midlatitudes shifts. J. Clim. 25, 4330–4347.
Schulz, N., Boisier, J.P., Aceituno, P., 2011. Climate change along the arid coast of northern Chile. Int. J. Climatol. 32 (12), 1803–1814. https://doi.org/10.1002/joc.2395.
Sifeddine, A., Gutiérrez, D., Ortlieb, L., Boucher, H., Velazco, F., Field, D., Vargas, G., Boussafir, M., Salvatteci, R., Ferreira, V., García, M., Valdés, J., Caquineau, S., Mandeng Yogo, M., Cetin, F., Solis, J., Soler, P., Baumgartner, T., 2008. Laminated sediments from the central Peruvian continental slope: a 500 year record of upwelling system productivity, terrestrial runoff and redox conditions. Prog. Oceanogr. 79, 190–197.
Stott, L., Cannariato, K., Thunell, R., Haug, G., Koutavas, A., Lund, S., 2004. Decline of surface temperature and salinity in the western tropical Pacific Ocean in the Holocene epoch. Nature 431, 56–59. https://doi.org/10.1038/nature02903.
Taylor, K.E., Stouffer, R.J., Meehl, G.A., 2012. An overview of CMIP5 and the experimental design. Bull. Am. Meteorol. Soc. 93, 485–498. https://doi.org/10.1175/BAMS-D-11-00094.1.
Vargas, G., Ortlieb, L., Pichon, J.J., Bertaux, J., Pujos, M., 2004. Sedimentary facies and high resolution primary production inferences from laminated diatomaceous sediments off northern Chile (23°S). Mar. Geol. 211, 79–99.
Vargas, G., Rutllant, J., Ortlieb, L., 2006. ENSO tropical–extratropical climate teleconnections and mechanisms for Holocene debris flows along the hyperarid coast of western South America (17°–24°S). Earth Planet. Sci. Lett. 249, 467–483.
Vargas, G., Pantoja, S., Rutllant, J.A., Lange, C.B., Ortlieb, L., 2007. Enhancement of coastal upwelling and interdecadal ENSO-like variability in the Peru–Chile current since late 19th century. Geophys. Res. Lett. 34, L13607. https://doi.org/10.1029/2006GL028812.
Vargas, G., Pérez, S., Aldunce, P., Aluviones y resiliencia en Atacama, 2018. Construyendo saberes sobre riesgos y desastres. Soc. Ediciones. http://www.libros.uchile.cl/838.
Veit, H., 1996. Sourthern Westerlies during the Holocene deduced from geomorphological and pedological studie in the Norte Chico, Northern Chile (27–33°S). Palaeogeogr. Palaeoclimatol. Palaeoecol. 123, 107–119.
Villagrán, C., Varela, J., 1990. Palynological evidence for increased aridity on the central Chilean coast during the Holocene. Quat. Res. 34, 198–207.
Villa-Martínez, R., Villagrán, C., Jenny, B., 2003. The last 7500 cal yr BP of westerly rainfall in Central Chile inferred from a high-resolution pollen record from Laguna Aculeo (34°S). Quat. Res. 60, 284–293.
Villa-Martinez, R., Villagrán, C., Jenny, B., 2004. Pollen evidence for late-Holocene climatic variability at Laguna de Aculeo, Central Chile (lat. 34°S). The Holocene 14 (3), 361–367.
Ward, P.J., Jongman, B., Kummu, M., Dettinger, M.D., Spema Weiland, F.C., Winsemius, H.C., 2014. Strong influence of El Niño Southern Oscillation on flood risk around the world. PNAS 111, 15659–15664.
Wilcox, A.C., Escauriaza, C., Agredano, R., Mignot, E., Zuazo, V., Otárola, S., Castro, L., Gironás, J., Cienfuegos, R., Mao, L., 2016. An integrated analysis of the March 2015 Atacama floods. Geophys. Res. Lett. 43, 8035–8043. https://doi.org/10.1002/2016GL069751.